In situ monitoring of orientation parameters and orientation distribution functions of polyethylenes during tensile tests

In situ monitoring of orientation parameters and orientation distribution functions of polyethylenes during tensile tests

*Yusuke Hiejima, Takumitsu Kida and Koh-hei Nitta**

Department of Chemical and Materials Science, Kanazawa University, Kakuma Campus, 920-1192 Kanazawa, Japan
Fax: (+81) 76 2344829; E-mail: nitta@se.kanazawa-u.ac.jp

Summary: *In situ* polarized Raman spectroscopy is applied for the tensile deformation of high- and low-density polyethylenes (HDPE and LDPE), and the orientation parameters as well as the orientation distribution function (ODF) are determined. While random orientation is maintained in the elastic region, the orientation of the polymer chains begins after the first yield point. The ODF for LDPE shows a peak at the stretching direction throughout the elongation process, and the maximum value of the ODF monotonously increases with the strain. For HDPE, the ODF in the yielding region has a broad peak at an intermediate angle of 30–70° from the stretching direction, while the orientation at the stretching direction is restored in the strain-hardening region. The tilted orientation is explained with the concept of the lamellar cluster units formed in the yielding region after the collapse of the spherulites. The HDPE with lower molecular weight and that with wider molecular weight distribution show high orientation, which is explained with the smaller size of the lamellar cluster units and the higher network density in the amorphous phase, respectively.

Keywords: rheo-Raman spectroscopy, polyethylene, orientation parameters, orientation distribution function, tensile deformation

Introduction

Polyolefin materials such as polyethylene (PE) are ubiquitous in our daily life. While the plastic products are commonly formed under deformation, it has been established that the mechanical properties of the polymeric solids are strongly affected by the molecular orientation. The orientation behaviors of polyethylenes including high- and low-density polyethylenes (HDPE and LDPE) have long been investigated by a variety of methods[1-7]. The wide-angle X-ray diffraction (WAXD) has been employed to reveal the orientation of the lamellar crystals[4,8]. The infrared (IR) spectroscopy has been utilized the orientation of the amorphous chains, as well as the crystalline chains[5-7] .

Polarized Raman spectroscopy has several advantages as a method of investigation for the orientation behaviors of polymeric materials[9]. While IR spectroscopy gives

orientation function which gives a measure of averaged orientation, two orientation parameters $<P_2>$ and $<P_4>$ are determined by polarized Raman spectroscopy. The combination of these two parameters such as the $<P_2>$–$<P_4>$ diagram[10-12] enable us to quantify the spatial alignment of molecular chain axis and the orientation distribution function (ODF)[13-15]. Since the pioneering works of the ODF by Bower[14] the methods of analysis for determing the ODF has been developed progressively[16-20].

In this work, *in situ* polarized Raman spectroscopy is employed for PE during uniaxial stretching. The orientation parameters $<P_2>$ and $<P_4>$ as well as the ODF are determined for HDPE and LDPE. The relation between the orientation behaviors and the molecular characteristics such as the molecular weight, the molecular weight distribution and the crystallinity are discussed.

Experimental

The pellets of HDPE, LDPE (Tosoh Corp., Japan) and MDPE (Prime Polymer Co. Ltd., Japan) were used. The pellets were melted and compressed at 210°C and 20 MPa for 5 min folowed by quenched in iced water. The sample sheet was anealed at specified temperature for 4 h to parepare a sheet with a thickness of approximately 1 mm. The characteristics of the PE sheets are listed in Table 1. The density was determined with the Archimedes method, and the crystallinity was calculated by assuming the densities of the crystalline and amorphous phases were ρ_c=1000 kg/m^3 and ρ_a=855 kg/m^3 [21], respectively. The SAXS measurements were performed by using a NanoViewer (Rigaku) with a CuKα

Table 1 Characteristics of PEs.

Sample code	M_w	M_w/M_n	T_a /°C [a)]	χ_v /% [b)]	L_c /nm [c)]
HDPE19_66	1.86×10^5	6.0	110	66	18.5
HDPE10_66	1.00×10^5	5.9	100	66	16.0
HDPE19_58	1.86×10^5	6.0	40	58	14.6
HDPE17_58	1.70×10^5	15.0	110	58	14.6
MDPE	1.70×10^5	15.0	40	54	13.4
LDPE	6.9×10^4	3.8	40	41	5.3

[a)] Annealing temperature.
[b)] Volumetric crystallinity.
[c)] Lamellar crystalline thickness.

radiation at 40 kV and 30 mA. The 2-D scattering patterns were acquired by using an imaging plate with an exposure time of 30 min. The lamellar crystalline thickness was estimated from the normalized linear correlation function which was calculated from the Fourier transform of the 1D radial intensity profile[22].

The experimental setup for the rheo-Raman spectroscopy has been described elsewhere[16,23-25], being described briefly. Laser light from a DPSS laser (Lasos, Germany) at a wavelength of 639.6 nm and a power of 200 mW was irradiated into the central portion of the specimen under stretching with a tensile tester. The double-drawing mechanism of the tensile machine enable us to keep the excitation light focused on the central portion of the specimen during the uniaxial stretching. The backward-scattered light was collected with a pair of convex lenses and detected with a CCD camera equipped with a spectrometer (PIXIS100 and SpectraPro 2300i, Princton Instruments). The tensile tests were conducted at 20°C at a constant elongation speed of 1 mm/min. The Raman spectra were accumulated for 10 times with an exposure time of 1 s.

The orientation parameters were determined from a set of polarized Raman spectra with three polarization geometries. The orientation parameters $\langle P_2 \rangle$ and $\langle P_4 \rangle$ defined as

$$\langle P_2 \rangle = \frac{3\langle \cos\theta \rangle - 1}{2}, \tag{1}$$

$$\langle P_4 \rangle = \frac{35\langle \cos^4\theta \rangle - 30\langle \cos^2\theta \rangle + 3}{8}, \tag{2}$$

were determined from the intensities of the 1130 cm^{-1} band assigned to the crystalline symmetric C-C stretching mode[11,12,23,26,27].

The ODF is a probability distribution function that a molecular chain orients toward a polar angle of θ from the stretching direction[11,14]. The Legendre expansion of ODF is written as

$$N(\theta) = \sum_{n=even}^{\infty} \frac{2l+1}{2} \langle P_n \rangle P_n(\cos\theta), \tag{3}$$

where $\langle P_n \rangle$ is the n-th moment and $P_n(x)$ is the n-th Legendre polynomial and the summation is taken for all terms of even orders. Since these moments of $N(\theta)$ are equivalent to the orientation parameters, the second and fourth moments $\langle P_2 \rangle$ and $\langle P_4 \rangle$ were determined from the experimental Raman spectra. The sixth and higher moments were estimated by maximizing the information entropy of molecular orientation[11]

$$S = -\int_0^{\pi} N(\theta) \ln N(\theta)\, d\theta, \tag{4}$$

where the integration is taken over the entire direction. The explicit form of $N(\theta)$ under the constraints of

$$\int_0^{\pi} N(\theta)\sin\theta\, d\theta = 1, \tag{5}$$

$$\int_0^{\pi} N(\theta)P_2(\cos\theta)\sin\theta\, d\theta = \langle P_2 \rangle, \tag{6}$$

$$\int_0^{\pi} N(\theta)P_4(\cos\theta)\sin\theta d\theta = \langle P_4 \rangle, \tag{7}$$

are deduced as

$$N(\theta) = \frac{\exp\left[\lambda_2 P_2(\cos\theta) + \lambda_4 P_4(\cos\theta)\right]}{\int_0^{\pi} \exp\left[\lambda_2 P_2(\cos\theta) + \lambda_4 P_4(\cos\theta)\right]\sin\theta d\theta}, \tag{8}$$

where λ_2 and λ_4 are the Legendre multiplyers[13,28,29].

The maximization of the information entropy given by Eqn. (4) also gives the most probable values of $<P_4>$ under a given value of $<P_2>$. It has been reported that the most-probable value $<P_4>_{mp}$ is approximately decribed by the polynomials of $<P_2>$ as

$$\langle P_4 \rangle_{mp} = -0.083\langle P_2 \rangle + 1.366\langle P_2 \rangle^2 - 1.899\langle P_2 \rangle^3 + 1.616\langle P_2 \rangle^4 \tag{9}$$

for positive $<P_2>$, and

$$\langle P_4 \rangle_{mp} = 0.052\langle P_2 \rangle + 1.574\langle P_2 \rangle^2 + 3.968\langle P_2 \rangle^3 + 8.058\langle P_2 \rangle^4 \tag{10}$$

for negative $<P_2>$ [18,29].

Results and discussion

In Fig. 1, the orientation parameters for PEs are shown along with the stress-strain curves. The overall orientation behaviors of HDPE are similar as shown in Fig. 1 (a)-(d). In the elastic region where the stress linearly increases with the strain, the both of $<P_2>$ and $<P_4>$ remain almost zero, indicating that the crystalline chains are randomly oriented. Beyond the first yield point at the maximum of the stress, $<P_2>$ begins to increase, indicating the onset of the crystalline chain orientation to the stretching direction. For HDPE, $<P_4>$ decreases with increasing the strain, and shows a minimum in the yielding region. The downward deviation of $<P_4>$ from $<P_4>_{mp}$ calculated by Eqns. (9) and (10) is a consequence of a tilted orientation toward an polar angle of θ=30–70° [12,16,23] instead of the stretching axis at θ=0°. The oblique orientation in the yielding region is explained by considering the existence of the lamellar cluster units[23]. Because the crystalline chains

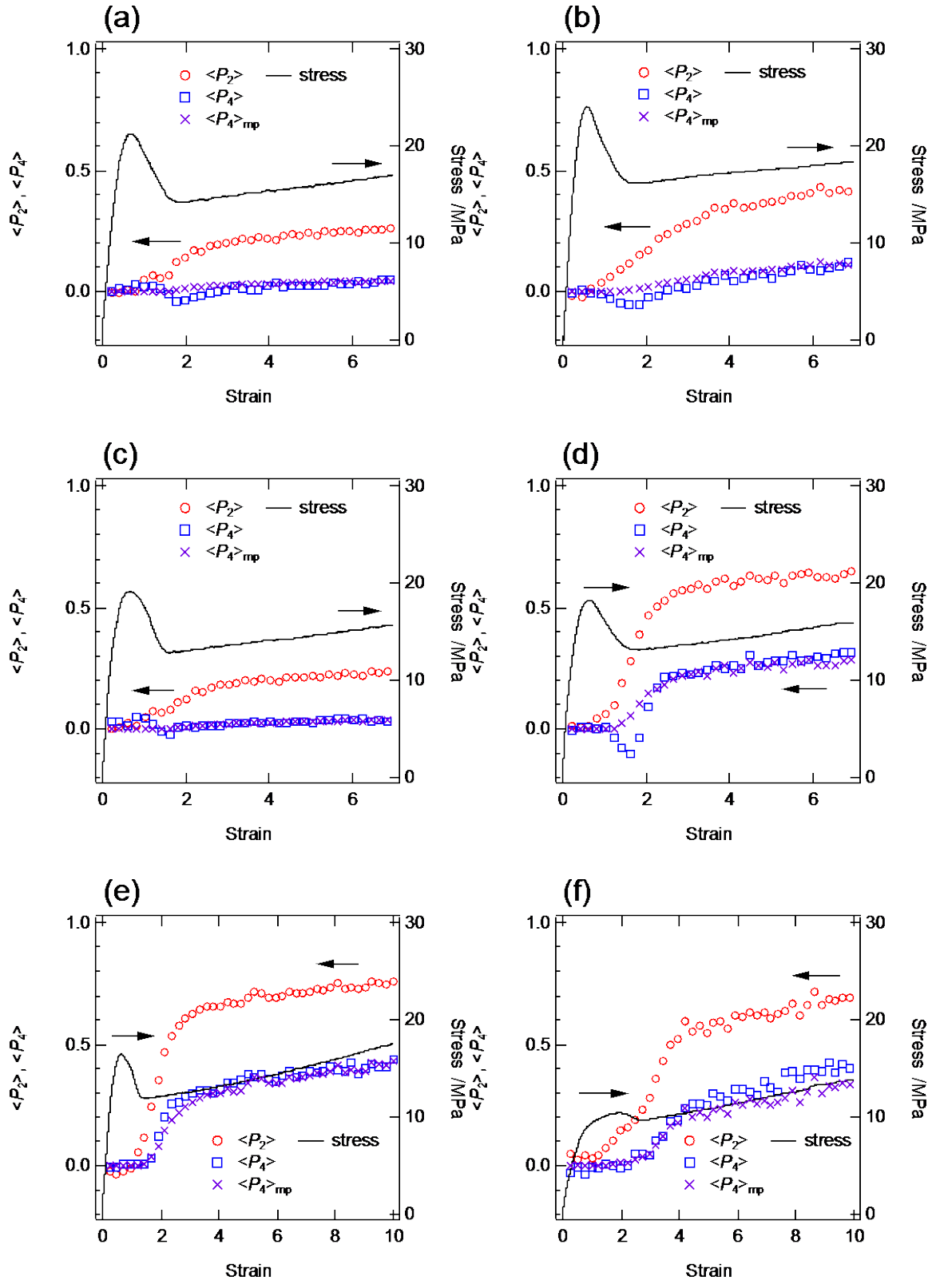

Fig. 1 Stress-stain curves and strain dependence of orientation parameters $\langle P_2 \rangle$ and $\langle P_4 \rangle$ for (a) HDPE19_66, (b) HDPE10_66, (c) HDPE19_58, (d) HDPE17_58, (e) MDPE and (f) LDPE. The most-probable values $\langle P_4 \rangle_{mp}$ calculated with Eqn. (9) is also plotted. (See Table 1 for the details of these sample codes.)

are contained in the lamellar cluster units which are formed by the fragmentation of the lamellar crystals after the collapse of the spherulites[30,31] , the molecular orientation is attained through rotational motions of the lamellar cluster units. Then, the orientation toward the stretching direction is hindered, because the bulky and rigid lamellar cluster units are densely packed in the yielding region[23,32]. In the strain-hardening region, the slopes of $<P_2>$ and $<P_4>$ become more gradual, suggesting that the orientation toward the stretching direction has been almost completed. The values of $<P_4>$ agrees well with the those of $<P_4>_{mp}$ beyond the yielding region, indicating the molecular orientation toward the stretching direction is restored in the strain-hardening region.

The effects of the molecular weight are investigated between HDPE19_66 and HDPE10_66 shown in Fig. 1 (a) and (b), where the crystallinity is set at the same value of 66%. The values of $<P_2>$ for HDPE19_66 are appreciably smaller than those of HDPE10_66, indicating that the orientation is suppressed with increasing the molecular weight. The M_w dependence is explained by the size of the lamellar cluster units which is proportional to $M_w^{1/2}$ [30,31]. Because the HDPE with lower molecular weight has smaller lamellar cluster units, the orientation toward the stretching direction is smoother, resulting in higher orientation. The enhancement of orientation is also attained by the increase of M_w/M_n, even if the M_w is essentially the same as shown in Fig. 1 (c) and (d). As shown in Table 1, the lamellar thickness is not affected M_w/M_n, suggesting that the effect of the molecular weight distribution can be attributed to the difference in the amorphous phase. Because the network density which would work as the stress transmitter[33–35] in the amorphous phase is expected to be higher in HDPE with higher M_w/M_n [36], the crystalline orientation through the rotation of the lamellar cluster units seems to be promoted, and higher orientation is achieved. This explanation is consistent with the fact that the effect of M_w/M_n is observed only in the strain-hardening region where the amorphous chains are predominant for the orientation behaviors[36].

Although the stress-strain curve of LDPE differs from those of HDPE with low crystallinity as shown in Fig. 1 (f), the orientation behaviors are similar; the orientation toward the stretching direction begins after the first yield point, and proceeds rapidly to reach highly-orientated states in the strain-hardening region. While a minimum of $<P_4>$ is observed for HDPE in the yielding region, $<P_4>$ for MDPE and LDPE monotoneously increases with the strain, and the values of $<P_4>$ are practically described by $<P_4>_{mp}$ during the entire tensile stretching. These orientation behaviors are similar to HDPE under hot drawing[24], where the onset of the intercrystalline relaxtion leads to smoother

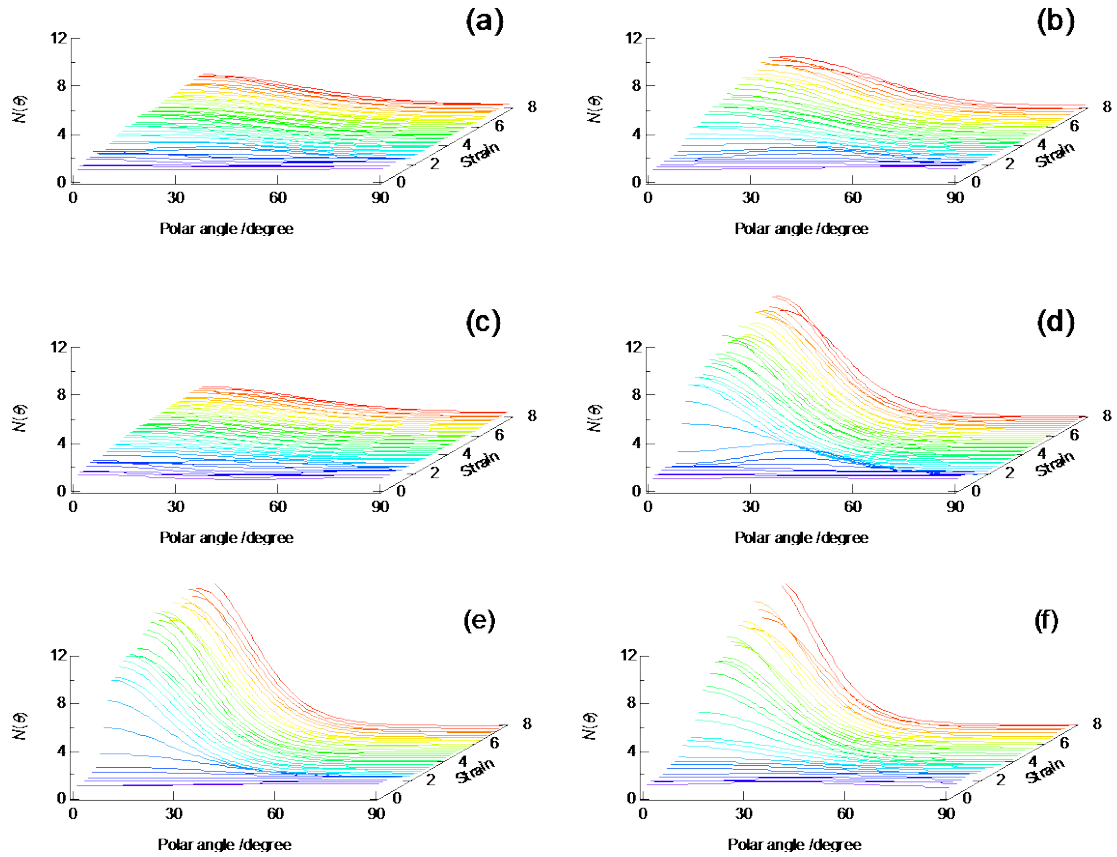

Fig. 2 Orientation distribution functions at various strains for (a) HDPE19_66, (b) HDPE10_66, (c) HDPE19_58, (d) HDPE17_58, (e) MDPE and (f) LDPE. (See Table 1 for the details of these sample codes.)

orientation toward the stretching direction. As shown in Table 1, the lamellar thickness of LDPE and MDPE are appreciably smaller than those of HDPE, then, the origin of the smoother orientation can be attributed to more fragile lamellar structures.

The orientation behavior of PE is visualized with the ODF as shown in Fig. 2. Before elongation, the ODF is constant irrespective of the polar angle. In the yielding region at ε~1.5 for HDPE, the ODF has a broad peak centered at θ=30–70°. The tilted orientation in the yielding region is clearly observed for HDPE where $\langle P_4 \rangle$ shows distinct deviation from $\langle P_4 \rangle_{mp}$. In the strain-hardening region, the ODF shows a prominent peak at the stretching direction (θ=0°), and the height of the peak increases with increasing the strain. For MDPE and LDPE, the ODF shows a prominent peak at θ=0° in the whole range of the strains, and the maximum of $N(\theta)$ monotoneously increases with the strain, indicating the orientation toward the stretching direction proceeds smoothly.

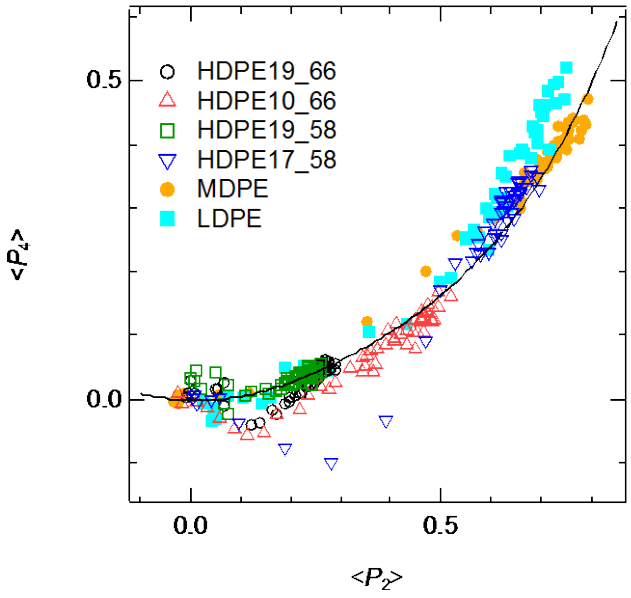

Fig. 3 $\langle P_2 \rangle$-$\langle P_4 \rangle$ plot for various PEs listed in Table 1. The solid curve represents the most-probable values calculated with Eqns. (9) and (10).

The orientation behaviors in various PEs are compared by plotting $\langle P_4 \rangle$ as a function of $\langle P_2 \rangle$ in Fig. 3. These values basically lie on a single curve, because the value of $\langle P_4 \rangle$ is approximately represented by the value of $\langle P_4 \rangle_{mp}$ given by Eqn. (9) and (10) except for the yielding region. The downward deviation of $\langle P_4 \rangle$ from $\langle P_4 \rangle_{mp}$ is obvious for HDPE, where the orientation toward the stretching direction is hindered by the formation of the rigid and bulky lamellar cluster units as the mobile units. Then, except for the yielding region of HDPE with highly crystalline nature, the orientation parameters $\langle P_2 \rangle$ is a good measure of the orientation, and the ODF is simply calculated as a most-probable distribution under the given value of $\langle P_2 \rangle$.

Conclusion

The orientation parameters and the orientation distribution functions are determined from the *in situ* Raman spectroscopy during uniaxial stretching of PE. While no orientation occurs in the elastic region, molecular orientation takes place in the yielding region which is observed as a sharp rise of $\langle P_2 \rangle$. A drop of $\langle P_4 \rangle$ and the tilted orientation toward an intermediate angle of θ=30–70° were observed in the yielding region. The hindrance of the orientation toward the stretching region was explained by the exisitence of bulky and rigid lamellar cluster units which was formed after the collapse of the spherulites. The values of $\langle P_2 \rangle$ at high strains depends on the molecular weight and the distribution; lower molecular weight and wide molecular weight distribution give higher

orientation. The value of $\langle P_4 \rangle$ is essentially the same as that of $\langle P_4 \rangle_{mp}$, except for the yielding region of HDPE, indicating that an ideal uniaxial orientation is attained in the strain-hardening region, where the ODF is simply evaluated solely with $\langle P_2 \rangle$. Since we found that the primary structures of polyethylenes such as the molecular weights (M_w and M_n) and the branched structures strongly affect the deformation behaviors, these effects are currently under investigation.

Acknowledgment

YH and TK are thankful to the financial support by JSPS KAKENHI (Grant Number 26410221) and JSPS Research Fellowships for Young Scientists (Grant Number 16J00528), respectively.

[1] E. F. Oleinik, *Polym. Sci. Ser. C*, **2003**, *45*, 17.
[2] H. Shinzawa, W. Kanematsu, I. Noda, *Vib. Spectrosc.*, **2014**, *70*, 53.
[3] M. Mizushima, T. Kawamura, K. Takahashi, K.-H. Nitta, *Polym. Test.*, **2014**, *38*, 81.
[4] Z. Jiang, Y. Tang, J. Rieger, H.-F. Enderle, D. Lilge, S. V. Roth, R. Gehrke, Z. Wu, Z. Li, Y. Men, *Polymer*, **2009**, *50*, 4101.
[5] Y. Song, A. K. -H. Nitta, N. Nemoto, *Macromolecules*, **2003**, *36*, 1955.
[6] H. Li, W. Zhou, Y. Ji, Z. Hong, B. Miao, X. Li, J. Zhang, Z. Qi, X. Wang, L. Li, Z.-M. Li, *Polymer*, **2013**, *54*, 972.
[7] M. Plass, R. Streck, J. Nieto, H. W. Siesler, *Macromol. Symp.*, **2008**, *265*, 166.
[8] R. Hiss, S. Hobeika, C. Lynn, G. Strobl, *Macromolecules*, **1999**, *32*, 4390.
[9] M. Tanaka, R. J. Young, *J. Mater. Sci.*, **2006**, *41*, 963.
[10] S. Nomura, N. Nakamura, H. Kawai, *J. Polym. Sci. A-2 Polym. Phys.*, **1971**, *9*, 407.
[11] D. I. Bower, *J. Polym. Sci. Polym. Phys. Ed.*, **1981**, *19*, 93.
[12] M. R-. Lacroix, C. Pellerin, *Macromolecules*, **2013**, *46*, 5561.
[13] B. J. Berne, *J. Chem. Phys.*, **1968**, *49*, 3125.
[14] D. I. Bower, *J. Polym. Sci. Polym. Phys. Ed.*, **1972**, *10*, 2135.
[15] D. I. Bower, *J. Polym. Sci. Polym. Phys. Ed.*, **1981**, *19*, 93.
[16] T. Kida, Y. Hiejima, K. -H. Nitta, *Express Polym. Lett.*, **2016**, *10*, 701.
[17] M. J. Citra, D. B. Chase, R. M. Ikeda, K. H. Gardner, *Macromolecules*, **1995**, *28*, 4007.
[18] F. L. Labarthet, T. Buffeteau, C. Sourisseau, *Appl. Spectrosc.*, **2000**, *54*, 699.
[19] S. Frisk, R. M. Ikeda, D. B. Chase, J. F. Rabolt, *Appl. Spectrosc.*, **2004**, *58*, 279.
[20] M. R-. Lacroix, C. Pellerin, *Appl. Spectrosc.*, **2013**, *67*, 409.
[21] J. Brandrup, E. H. Immergut, E. A. Grulke, A. Abe, D. R. Bloch, *"Polymer Handbook" 4th Edition*, Wiley, New York 1999.
[22] G. R. Strobl, M. Schneider, *J. Polym. Sci. Polym. Phys. Ed.*, **1980**, *18*, 1343.
[23] T. Kida, T. Oku, Y. Hiejima, K.-H. Nitta, *Polymer*, **2015**, *58*, 88.
[24] T. Kida, Y. Hiejima, K.-H. Nitta, *Polym. Test.*, **2015**, *44*, 30.
[25] T. Kida, Y. Hiejima, K.-H. Nitta, *Int. J. Experim. Spectrosc. Tech.*, **2016**, *1*, 1.
[26] M. Pigeon, R. E. Prud'homme, M. Pezolet, *Macromolecules*, **1991**, *24*, 5687.
[27] D. I. Bower, *J. Polym. Sci. Polym. Phys. Ed.*, **1972**, *10*, 2135.
[28] M. Tanaka, R. J. Young, *J. Macromol. Sci. B*, **2005**, *B44*, 967.

[29] H. Pottel, W. Herreman, B. W. van der Meer, M. Ameloot, *Chem. Phys.*, **1986**, *102*, 37.
[30] K.-H. Nitta, M. Takayanagi, *J. Macromol. Sci. B*, **2003**, *42*, 107.
[31] M. Takayanagi, K.-H. Nitta, O. Kojima, *J. Macromol. Sci. B*, **2003**, *42*, 1049.
[32] M. Kuriyagawa, K.-H. Nitta, *Polymer*, **2011**, *52*, 3469.
[33] K.-H. Nitta, M. Takayanagi, *J. Polym. Sci. Part B Polym. Phys.*, **1999**, *37*, 357.
[34] R. Seguela, *J. Polym. Sci. Part B Polym. Phys.*, **2005**, *43*, 1729.
[35] Y. Men, J. Rieger, G. Strobl, *Phys. Rev. Lett.*, **2003**, *91*, 95502.
[36] B. A. G. Schrauwen, R. P. M. Janssen, L. E. Govaert, H. E. H. Meijer, *Macromolecules*, **2004**, *37*, 6069.